WOOD RESEARCH
64 (2): 2019
223-236

AXIAL COMPRESSIVE CREEP BEHAVIOUR OF A SQUARE STEEL TUBE/BAMBOO PLYWOOD COMPOSITE COLUMN WITH BINDING BARS

Weifeng Zhao
Guangdong Construction Polytechnic
Guangzhou, China

Weifeng Zhao, Bin Yang
Xiangtan University, College of Civil Engineering and Mechanics
Xiangtan, China

Jing Zhou
South China University of Technology, Key Laboratory of Subtropical Architecture Science
Guangzhou, China

(Received May 2018)

ABSTRACT

Four specimens of a thin-walled square steel tube/bamboo plywood composite hollow column with binding bars (SBCCB) were each subjected to an axial compressive creep test and a subsequent axial compression test to examine their axial compressive creep behavior and post-creep compressive failure modes as well as to analyze the effects of long-term loading on the ultimate axial compression-bearing capacity of the SBCCB. The results show that the axial compressive creep strain decreased with increasing slenderness ratio and increased with increasing axial compressive stress. The creep–time curves of the specimens with various slenderness ratios all exhibited a transient creep stage and a steady-stage stage. Temperature and humidity variations affected local creep behavior. Creep significantly affected the axial compression-bearing capacity as well as the axial and lateral deformability of the SBCCB. The rheological mechanics-based Burgers model can well predict the creep strain development of the SBCCB.

KEYWORDS: *Bambusoideae*, bamboo plywood, thin-walled square steel tube, composite hollow column, axial compressive creep, post-creep bearing capacity.

INTRODUCTION

Bamboo is an important fast-growing and renewable forest resource. The tensile and compressive strengths of the outer part of 5~8 year-old bamboo material are approximately 2 and 1.5 times those of timber (Liu et al. 2013), respectively. The specific strength of bamboo is also higher than that of most timber and ordinary steel products (Bathtiar et al. 2013). Raw bamboo products, such as raw bamboo scaffolds and railings and simple raw bamboo shed frames, have been used in numerous fields, e.g., construction and transportation (Sharma et al. 2015). In Colombia, Trujillo et al. (2013) notes five types of bamboo structures: traditional construction, social housing, luxury housing, long-span buildings and footbridges. However, raw bamboo materials are hollow and have thin walls and relatively small diameters with significantly variable geometric sizes and mechanical properties. While there are more than 1200 species worldwide (Ramage et al. 2015), full culm bamboo construction is limited by the variation in geometric and mechanical properties. The difficulty in making connections and joints suitable for round (and variable) sections is also prohibitive for mainstream construction. Therefore, raw bamboo materials are unable to meet the mechanical and component-size requirements for modern engineering structures. Laminated bamboo composite engineering materials are one of the most feasible applications of bamboo resources (Sharma et al. 2015, Ramage et al. 2015). However, applications of laminated bamboo materials in engineering have focused on concrete-based construction, and research on using laminated bamboo materials as an engineered structural material has only been conducted recently (Xiao et al. 2010, Li et al. 2014b, Li et al. 2015). Significant progress has been made in the studies and applications of bamboo composite materials and bamboo-laminated materials (Li et al. 2015, Verma and Chariar 2012), including steel/bamboo plywood composite structural columns (Zhao et al. 2016a, Zhang et al. 2015). With the increasing shortage of engineered wood and the promotion of sustainable green construction materials, research on steel/bamboo composites has received significant attention worldwide. With the successful development of laminated bamboo materials, steel/bamboo composite structural elements have been developed in recent years in China. Liu et al. (2013) developed a bamboo structural box column with bamboo plywood and L-shaped steel, and Li et al. (2014a) investigated a bamboo composite column reinforced by steel rebar. Xie et al. (2012) proposed a C-shaped thin-walled steel/bamboo plywood composite box column and studied its creep behaviour under compressive and long-term loading. Zhao et al. (2016b) developed a thin-walled square steel tube/bamboo plywood composite hollow column (SBCC). On this basis, to effectively hamper interfacial adhesion failures, Zhao et al. (2016a, 2018) developed a SBCC with binding bars (SBCCB) and studied its axial and eccentric compressive strengths. The thin-walled steel tube in the column served as the skeleton, which made the composite suitable for industrial assembly, and increased the cross-sectional area of the composite columns, thereby reducing the slenderness ratio and effectively improving the instability and failure performance of the columns under pressure. Transverse binding bars were used to ensure the composite effect of the bamboo/steel composite column, which effectively reduced the debonding failure, changed the limiting damage mode, and significantly improved the load bearing capacity of the SBCCB.

The phenomenon of bamboo creep, which can result in greater deformation and earlier failure of structural elements, is critical to structural design. Many studies have investigated the creep behavior of bamboo-based products in bending (Ma et al. 2017, Li and Xiao 2016, Gottron 2014, Xiao et al. 2014, Amino 2005), however, few studies have examined the creep behavior of bamboo-based products in compression. In this study, the short-term axial loading tests of the SBCCBs are examined (Zhou et al. 2018). Four SBCCB specimens with slenderness ratios

varying from 40 to 70 were each subjected to a long-term (120-day) axial compressive creep test and a subsequent axial compression test to examine their compressive creep behavior, failure modes and characteristics as well as to analyse the effects of long-term loading on the ultimate compression-bearing capacity of the SBCCB.

MATERIAL AND METHODS

Specimen design and fabrication

Tab. 1 summarizes the specimen parameters. Fig. 1 shows the cross-sectional form of the specimens as well as the photographs of the finished specimens. The bamboo plywood used to prepare the specimens was cut from Moso bamboo mat plywood (2440 × 1220 × 10 mm) of the same batch and had a water content of 9%.

Tab. 1: Parameters of specimens.

Specimen number	Slenderness ratio λ	Sectional size $B \times B$ (mm)	Steel-tube $b \times b \times t$ (mm)	Loading level P_u(kN)	Spacing ratio of binding bars	Length (mm)
Z1	40	80×80	40×40×1.5	0.7Pu = 93.8	2.5	1033
Z2	50	80×80	40×40×1.5	0.6Pu = 70.8	2.5	1291
Z3	60	80×80	40×40×1.5	0.6Pu = 61.8	2.5	1549
Z4	70	80×80	40×40×1.5	0.6Pu = 53.7	2.5	1807

Note: Pu was calculated based on the equation for calculating the ultimate bearing capacity presented in reference (Li and Xiao 2016).

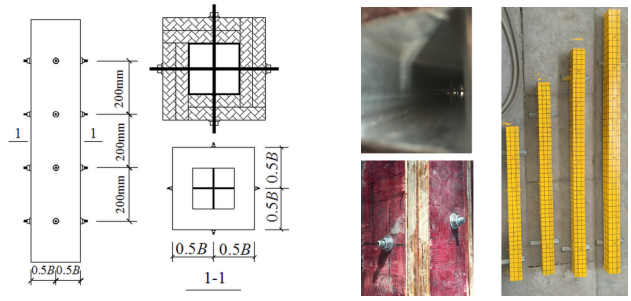

(a) *(b)*

Fig. 1: (a) Arrangement of binding bars and combination mode, (b) finished specimens.

Using standard test methods (GB/T 13123 2003), the transverse compressive elastic modulus, longitudinal compressive elastic modulus and longitudinal compressive strength of the bamboo plywood were determined to be 7.4, 8.3 and 24 GPa, respectively. Q235 galvanized seamless square steel tubes with an elastic modulus of 205 GPa, a yield strength of 260 MPa and an ultimate strength of 340 MPa were used to produce the thin-walled steel tube component. In addition, Ø6-mm fully threaded screws with yield strength of 260 MPa were used as the binding bars. For each specimen, the thin-walled steel tube was designed to be shorter than the bamboo plywood by 15-20 mm at each end and, together with the transverse binding bars, create a hooping effect, thereby preventing it from directly bearing the load. It has been demonstrated that 1.5 mm thickness of the thin-walled steel tube is sufficient for the thin-walled steel tube to ensure the composite effect of the column (Zhao et al. 2016a). A modified epoxy resin adhesive

with a shrinkage ratio below 1%, a tensile strength greater than 10 MPa and a shear strength greater than 12 MPa was selected as the interfacial adhesive. After fabrication, the assembled composite column specimens were fixed with clamps and cured for 7 to 10 days in a ventilated and dry environment to ensure that the adhesive reached its full bonding strength.

Creep test apparatus and measurement scheme

Due to the lack of a suitable creep test apparatus, a spring-type creep test apparatus was developed (Fig. 2) based on the creep test apparatuses used in another study (Cao and Fang 2005). The structure of this apparatus consisted of three sections: the top section consisted of a hydraulic jack and a pressure transducer, the loading test specimen was placed in the middle section, and a reaction spring was placed in the bottom section.

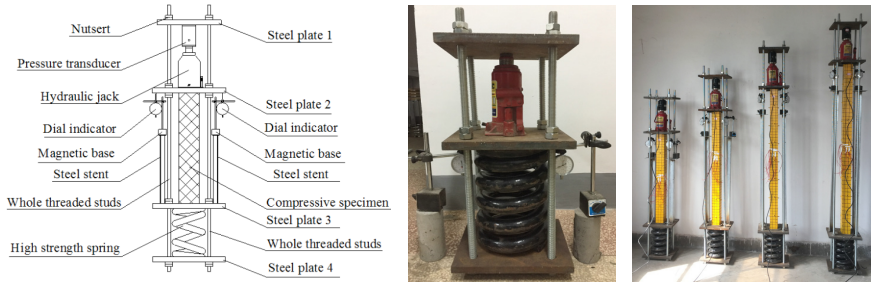

(a) *(b)* *(c)*

Fig. 2: (a) Test apparatus, (b) load maintenance test, (c) picture of actual loading.

To prevent unloading after the start of the loading process resulting from a loose apparatus, double nuts were used to tighten the apparatus. The spring used in the apparatus was a high-strength spring made of $60Si_2Mn$. A with properties specified in the Chinese National Standard GB/T 1222 (2016) with a wire diameter of 45 mm, a mean diameter of 180 mm, 4.5 active coils, a free length of 360 mm, a stiffness of 1.543 $N \cdot mm^{-1}$ and a maximum compression of 76 mm. The long-term compressive deformation of the specimen was measured using dial gauges with a measuring range of 5 mm. One dial gauge was placed at each side of the support steel frame. To test the capacity of the loading device to maintain a load, a simple measuring device was prepared with a hydraulic jack and the high-strength compression spring (Fig. 2(c)). Two dial gauges with a measuring range of 1 mm, one at each side of the device, were used to measure the capacity of the spring to maintain a constant load. The test lasted for 10 days. Tab. 2 summarizes the test data. The test results indicated that the loading device performed well in maintaining a load and could meet the creep test requirements.

Tab. 2: Load maintenance test data.

Time (d)	Left dial indicator reading (mm)	Left displacement variation (mm)	Right dial indicator reading (mm)	Right displacement variation (mm)
0	0.550	0	0.550	0
2	0.545	-0.005	0.550	0
4	0.547	0.002	0.548	-0.002
6	0.543	-0.004	0.545	-0.003
8	0.540	-0.003	0.542	-0.003
10	0.540	0	0.542	0
Total variation		-0.007		-0.003

After the axial pressure applied by the hydraulic jack reached the predetermined initial load, the nuts on the top of the steel plates in the middle section were tightened. After the initial loading was complete, the initial deformation of each specimen was recorded. Data were recorded once every 15 min for one hour after the initial loading, every three hours between the first and 10th hours after the initial loading and every four hours between the 10th hour and the second day after the initial loading. Afterwards, a middle- to long-term observation period began, during which data were recorded once every 12 hours between the fourth and 30th days, every 24 hours between the 30th and 60th days and every 48 hours between the 60th and 120th days.

Axial compression test apparatus and measurement scheme

The specimens subjected to the creep test were each subsequently subjected to a mechanical failure test, which was conducted after the specimens were unloaded and allowed to remain still for 10 days. Another specimen, which was called C4 (the design parameters for specimens C4 and Z4 were the same), was only subjected to the axial compression test according to GB/T 50329 (2002). Fig. 3 shows the test apparatus and the arrangement of the measurement points. Each specimen was fixed with a unidirectional knife hinge at each end to ensure that the specimen was loaded in the axial direction. Displacement sensors for measuring lateral deflection were placed on two adjacent sides in the middle of the specimen at the same height.

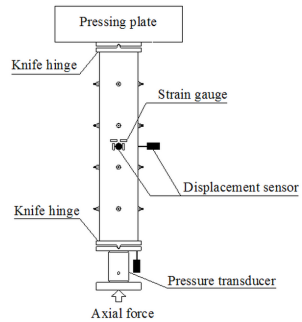

Fig. 3: Apparatus for the subsequent axial compression test.

Two rows (one in the transverse direction and one in the longitudinal direction) of strain gauges (two in each row) were placed on each side of the specimen. A displacement sensor was also placed at the bottom surface of the steel plate at the bottom of the column. The axial load and displacement data, as well as the axial and transverse strain data, were all collected using a static test system. The specimen was subjected to a multi-stage, slow, continuous and uniform displacement loading process. The test was terminated when the specimen had cracked relatively significantly or when significant unloading had occurred.

RESULTS AND DISCUSSION

Creep test results and analysis

The four specimens were tested for 120 days in a closed, indoor environment. During the test, the daily mean maximum and minimum temperatures were 22 and 5°C, respectively, i.e., a 17°C variation. In addition, the maximum and minimum indoor humidity levels were 88% and 50%, respectively, i.e., a 38-percentage-point variation. Fig. 4 shows the temperature and

moisture content variations. Since the temperature and moisture content varied to relatively small extents, to simplify the subsequent theoretical modeling process, the effects of temperature and humidity variations on the test results were not taken into consideration.

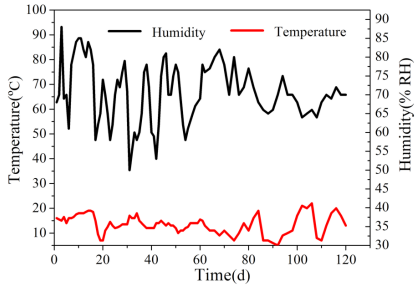

Fig. 4: Temperature and humidity variations.

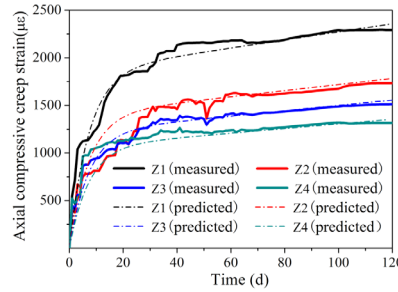

Fig. 5: Comparison of the measured and predicted creep strains.

During the creep test, the loading system was able to maintain a constant load. The strain of each specimen increased relatively rapidly in the initial stage of loading and then at a gradually decreasing rate. No failure was observed in specimens Z1, Z2 and Z3, whereas buckling was observed in specimen Z4, a specimen with a relatively large slenderness ratio, at the late stage of the test. During the whole test process, the binding bars performed well without undergoing noticeable bending or shear deformation. Fig. 5 shows the axial compressive creep strain-time curves. The following characteristics of the axial creep can be derived from the creep strain-time curves.

(1) A transient creep stage and a steady-state creep stage can be found in the axial compressive creep strain–time curve of each specimen. The transient creep stage lasted for approximately 20 days and varied significantly with the slenderness ratio. During the steady-state creep stage, the axial compressive creep strain of each specimen increased slowly. The same trend was observed in the strains of the four specimens. Because the load was approximately 0.3–0.4P_u lower than the predicted ultimate load, no creep failure stage was observed.

(2) The test was not conducted in a constant-temperature, constant-humidity environment. As a result, clear saw-tooth fluctuations were observed in the test curves. For example, the strain of specimen Z2 decreased significantly between the 50th and 60th days, which is an abnormal phenomenon caused by the sudden decrease in temperature, indicating that temperature and humidity affected short-term creep behavior to some extent.

(3) The same axial compressive load ratio (0.6P_u) was used to test specimens Z2, Z3 and Z4. The creep strain decreased with increasing slenderness ratio. The greater the slenderness ratio was, the smaller the corresponding creep strain. A comparison of the specimens at the same time (on the 80th day) revealed that the micro-strain of specimen Z2 (λ=50) reached 1,630; which was greater than that (1,440) of specimen Z3 (λ=60) and that (1,275) of specimen Z4 (λ=70). (4) The load level (0.7Pu) on specimen Z1 was higher than that (0.6P_u) on each of the other specimens. At the steady-state creep stage, the increase in the creep strain of specimen Z1 relative to specimen Z2 (4.3×10^{-4} – 7.97×10^{-4}) was greater than that of specimen Z2 relative to specimen Z3 (2.98×10^{-5} – 2.28×10^{-4}) and that of specimen Z3 relative to specimen Z4 (8.21×10^{-7} – 1.97×10^{-4}). These results indicate that the load level significantly affected creep development. A higher the load level resulted in greater creep, i.e., the creep increased gradually with increasing axial compressive stress level.

Axial compression test results and analysis

At the beginning of the loading process, the axial displacement of each specimen increased linearly with increasing axial load, and the specimen was in an elastic stage. When the load reached a certain level, microcracks began to appear at the adhesion interface between the substrate and the steel tube at the ends or centre of the column, accompanied by a slight cracking sound. As the load continued to increase, the cracks further propagated, and the cracking sound became louder; in addition, the adhesion interface cracked open, and the axial compressive deformation and transverse deflection of the specimen increased. As the load approached the ultimate load, the cracks propagated rapidly until the specimen failed. During the whole loading stage, the binding bars exhibited excellent mechanical performance without buckling or rupture. The damage characteristics of the four specimens are similar to the damage of other compression specimens without creep test (Zhao et al. 2016a). The profiles of the specimens after failure are shown in Fig. 6.

(a) *(b)* *(c)* *(d)*

Fig. 6: The profiles of the specimens after axial compression failure: (a) crushing failure of the bamboo plywood material at the column ends for Z1, (b) partial debonding failure of the adhesion interface on the side for Z2, (c) partial debonding failure of the adhesion interface on the side for Z3, and (d) buckling instability failure for Z4.

Fig. 7 shows the curves of the axial compressive load–axial displacement/strain and the axial compressive load–transverse displacement/strain (in the middle of the column). The ultimate bearing capacity decreased with increasing slenderness ratio. Under the same load, the axial and lateral displacements increased gradually with an increasing slenderness ratio. A greater slenderness ratio indicated a shorter linear elastic stage and the specimen entered the elastic-plastic stage earlier.

To determine the effects of long-term loading-induced creep on the ultimate bearing capacities of the specimens, specimen Z4, which was subjected to the 120-day creep test and the subsequent axial compression test, and specimen C4, which was only subjected to the axial compression test, were compared. The long-term loading-induced creep reduced the ultimate bearing capacity of the specimen.

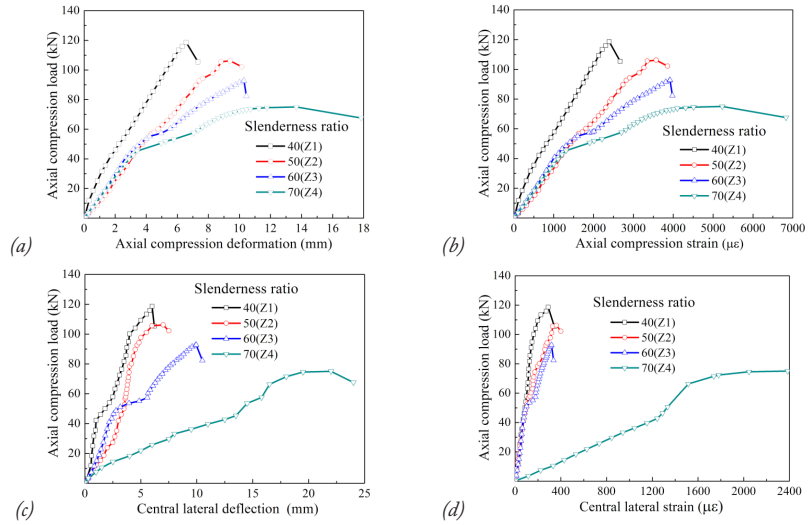

Fig. 7: Results of the subsequent axial compression tests: (a) load–axial deformation, (b) load–axial strain, (c) load–lateral deflection, (d) load–lateral strain.

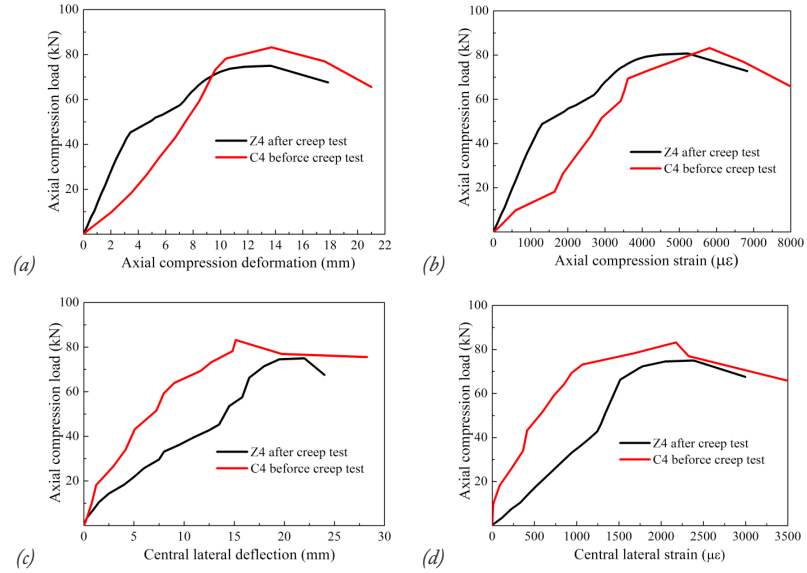

Fig. 8: Comparisons of the compression test results of specimens Z4 and C4: (a) comparison of the load–axial deformation results, (b) comparison of the load–axial strain results, (c) comparison of the load–lateral deflection results, (d) comparison of the load–lateral strain results.

The comparison of the test data shows that under a load of 0.6Pu, the ultimate bearing capacity of specimen Z4 decreased by approximately 9.8% after the 120-day creep test. The comparison of specimens Z4 and C4 (Fig. 8) shows that the axial load–displacement and axial

load–strain curves of the specimen before and after the long-term creep test had similar trends, but the maximum axial strain and displacement of the specimen as well as the transverse strain and displacement in the middle of the column decreased by varying amounts.

Tab. 3: Maximum deformation before and after creep.

Specimen number	Maximum axial displacement (mm)	Maximum axial strain (με)	Maximum central lateral deflection (mm)	Maximum central lateral strain (με)
Z4	17.84	6830.00	24.00	2994.05
C4	21.00	8024.70	28.24	3523.83

Tab. 3 shows the comparison of the test data. Long-term creep significantly affected the deformability of the SBCCB. Specifically, after the long-term compressive loading (creep) test, the SBCCB sustained plastic deformation. Because it was unable to recover from plastic deformation, a significant decrease in the deformability of the SBCCB was found in the subsequent compression test.

Based on an equation for calculating the ultimate bearing capacity that was derived from the axial compression test data of specimens that had not been subjected to creep tests (Zhou et al. 2018), the ultimate bearing capacities of the other specimens that were not subjected to creep tests were calculated, and the results were compared with the ultimate bearing capacities of the specimens that had been subjected to creep tests.

Tab. 4: Ultimate bearing capacities of the SBCCB specimens before and after the creep tests.

Specimen number	Slenderness ratio λ	Sectional size $B\times B$ (mm)	Steel-tube size $b\times b\times t$ (mm)	Loading level P(kN)	Ultimate bearing capacity before creep P_u(kN)	Ultimate bearing capacity after creep P_u'(kN)	P_u'/P_u
Z1	40	80×80	40×40×1.5	$0.7P_u$= 93.8	134.0	118.6	0.885
Z2	50	80×80	40×40×1.5	$0.6P_u$= 70.8	118.0	106.4	0.902
Z3	60	80×80	40×40×1.5	$0.6P_u$= 61.8	101.0	92.8	0.919
Z4	70	80×80	40×40×1.5	$0.6P_u$= 53.7	83.2	75.0	0.901

Tab. 4 summarizes the comparison results. After the creep test, the ultimate bearing capacity (P_u') decreased significantly (by 8.1–9.8% under a load of $0.6P_u$ and by 11.5% under a load of $0.7P_u$). The decrease in the ultimate bearing capacity of the specimens after the long-term creep test indicates that creep significantly affected the ultimate bearing capacity of the SBCCB. Thus, the effects of creep should be fully considered when using the SBCCB in engineering applications. Notably, the test did not consider the effect of the length of the loading period on the reduction in the material strength which warrants further investigation.

Creep deformation calculation

The phenomenon in which the deformation of a material slowly increases over time under a constant stress is referred to as creep, which can be described by a time function related to a viscoelastic rheological model. For the steel/bamboo composite column tested in this study, the bamboo was the main body that bore the compressive load, whereas the binding bars and the inner steel tube only created a hoop effect that prevented adhesion failures. Therefore, the bamboo plywood was the main body that underwent creep. In addition, the elastic modulus

of steel is far greater than that of bamboo. In the composite column, the creep of the steel was negligible compared to that of the bamboo. Bamboo is a typical viscoelastic biomass material and has properties between those of an ideal elastic material and those of an ideal viscous material. Thus, a mechanical model consisting of ideal elastic and viscous elements is suitable to characterize bamboo (Wu 2015). Ideal elasticity can be represented by a spring with an elastic modulus E_m as the characteristic parameter, whereas ideal viscosity can be represented by a damper or a viscous cylinder with a viscous modulus η_m as the characteristic parameter.

The Burgers model, which is a four-element model established by connecting the Maxwell model and the Kelvin model in series (Wu 2015), is often used to describe pre-tertiary stage creep curves. According to the Burgers model, at time t, the total strain of the SBCCB consisted of the transient elastic deformation described by the single elastic element in the Maxwell model, the viscous flow described by the single viscous element in the Maxwell model and the viscoelastic deformation described by the Kelvin model. Thus, the Burgers model of the SBCCB consisted of an elastic element and a viscous element connected in parallel (Fig. 9).

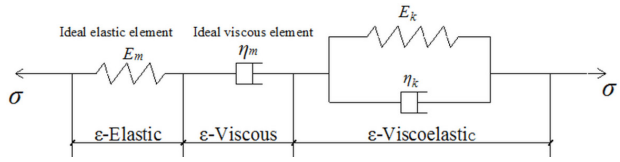

Fig. 9: Schematic diagram of the Burgers model.

Because the creep test conducted in this study did not involve the tertiary creep stage, the Burgers model could be used to describe the axial compressive creep behavior of the SBCCB specimens. The constitutive equation of the Burgers model is as follows:

$$\sigma+(\frac{\eta_m}{E_m}+\frac{\eta_k+\eta_m}{E_k})\dot{\sigma}+\frac{\eta_k\eta_m}{E_kE_m}\ddot{\sigma}=\eta_k\dot{\varepsilon}+\frac{\eta_k\eta_m}{E_k}\ddot{\varepsilon} \tag{1}$$

where: E_m and η_m - the characteristic parameters of the spring and viscous cylinder in the Maxwell model, respectively;
E_k and η_k - the characteristic parameters of the spring and viscous cylinder in the Kelvin model, respectively,
σ and ε - the total stress and total strain of the Burgers model, respectively.

For creep, a second-order constant coefficient nonhomogeneous linear differential equation with respect to ε can be obtained by substituting $\sigma=\sigma_0$ (t ≥ 0) into Eq. 1:

$$\sigma_0=\eta_k\dot{\varepsilon}+\frac{\eta_k\eta_m}{E_k}\ddot{\varepsilon} \tag{2}$$

Based on the initial condition, ,

$$\varepsilon(\mathrm{t})=\frac{\sigma_0}{E_m}+\frac{\sigma_0}{E_k}\left(1-e^{-\frac{E_k t}{\eta_k}}\right)+\frac{\sigma_0}{\eta_m}t \tag{3}$$

When the initial strain is not considered, the creep strain can be expressed as follows:

$$\varepsilon(\mathrm{t})=\frac{\sigma_0}{E_k}\left(1-e^{-\frac{E_k t}{\eta_k}}\right)+\frac{\sigma_0}{\eta_m}t \tag{4}$$

The undetermined parameters were obtained through nonlinear fitting using the test data, based on which the calculation model was determined. The reasonableness of the calculation model was preliminarily verified based on the creep strain calculated using the prediction model. The values of the parameters estimated by fitting were as follows: E_k=10,546.118 MPa, η_k=75,959.227 MPa·s, and η_m=4,594,571.827 MPa·s. The value of the overall correlation coefficient R^2=0.946. Fig. 4 shows the comparison of the predicted and measured values. The predicted values of the parameters of the four SBCCB specimens were in good agreement with the measured values, indicating that the Burgers model is highly capable of predicting the creep strain development of the SBCCB.

CONCLUSIONS

This study conducted experimental investigations of the performance of SBCCB specimens in compression. The following conclusions were drawn from the results.

The axial compressive creep strain of the SBCCB decreased with an increasing slenderness ratio and increased with an increasing axial compressive stress level. Similar variation trends were found in the axial compressive creep–time curves of the specimens with various slenderness ratios. The axial compressive creep–time curve of each specimen exhibited a typical transient creep stage and a typical steady-state stage. At the late stage of the creep test, the creep strain of each specimen increased slowly. Temperature and humidity variations affected the local creep behavior.

Long-term loading (creep) significantly affected the axial compression-bearing capacity of the SBCCB. The ultimate bearing capacity of the specimens that had been subjected to the axial compressive creep test and the subsequent axial compression test was 8.1–11.5% lower than that of the corresponding specimens that had only been subjected to the axial compressive creep test. After the long-term creep test, the specimens sustained permanent plastic deformation, and their axial and transverse deformability decreased significantly. The rheological mechanics-based Burgers model was highly capable of predicting the creep development of the SBCCB under long-term constant axial loading.

ACKNOWLEDGMENTS

The authors acknowledge the financial support from the National Natural Science Foundation of China (51708476 and 51708205), the Natural Science Foundation of Guangdong Province (2017A030310579), the Science and Technology Planning Project of Guangzhou City (201904010108), and the Department of Education of Guangdong Province (2017GKTSCX013).

REFERENCES

1. Amino, Y., 2005: Bamboo-precocious wood composite beams: bending capacity for long-term loading. Journal of Bamboo and Rattan 4(1): 55-70.
2. Bathtiar, E.T., Nugroho, N., Surjokusumo, S., Karlinasari, L., 2013: Eccentricity effect on bamboo's flexural properties. Journal of Biological Sciences 13(2): 82-87.

3. Cao, G.H., Fang, Z., 2005: Development and application of creep loading equipment. Research and Exploration in Laboratory 24(10): 31-33.
4. GB/T 13123, 2003: Standard test methods for bamboo-mat plywood.
5. GB/T 1222, 2016: Spring steels.
6. GB/T 50329, 2002: Standard for methods testing of timber structures.
7. Gottron, J., Harries, K.A., Xu, Q.F., 2014: Creep behavior of bamboo. Construction and Building Materials 66: 79-88.
8. Li, H.T., Su, J.W., Zhang, Q.S., 2015: Mechanical performance of laminated bamboo column under axial compression. Composites Part B: Engineering 79: 374-382.
9. Li, L., Xiao, Y., 2016: Creep behavior of glubam and CFRP-enhanced glubam beams. Journal of Composites for Construction 20(1): 04015028.
10. Li, Y., Chen, S.T., Meng, X., 2014a: Compressive strength test on bamboo column reinforced by clamps. China Forestry Science and Technology 28(4): 113-115.
11. Li, Z., Xiao, Y., Wang, R., Shan, B., 2014b: Experimental studies of light-weight wood frame shear walls with ply-bamboo sheathing panels. Journal of Building Structures 34(9): 142-149.
12. Liu, X., Yu, Y.S., Zhou, W.H., 2013: Study on compression resistance of bamboo building structural column. Journal of Central South University of Forestry & Technology 33(1): 104-108.
13. Ma, X.X., Smith, L.M., Wang, G., 2017: Mechano-sorptive creep mechanism of bamboo-based products in bending. Wood and Fiber Science 49(3): 277-284.
14. Ramage, M., Sharma, B., Bock, M., Mulligan, H., 2015: Engineered bamboo: state of the art. Proceedings of the Institution of Civil Engineers, Construction Materials 168(2): 57-67.
15. Sharma, B., Gatóo, A., Bock, M., 2015: Engineered bamboo for structural applications. Construction and Building Materials 81: 66-73.
16. Trujillo, D.J.A., Ramage, M., Change, W., 2013: Lightly modified bamboo for structural applications. Proceedings of the Institution of Civil Engineers, Construction Materials 166(4): 238-247.
17. Verma, C.S., Chariar, V.M., 2012: Development of layered laminate bamboo composite and their mechanical properties. Composites Part B: Engineering 43(3): 1063-1069.
18. Wu, B.Z., 2015: Experiment and analysis on creep properties of reconsolidated bamboo. PhD Thesis. Northeast Forestry University, Nanjing, China.
19. Xie, Q.T., Zhang, W.L., Jiang, T.Y., 2012: Experimental study on performance of steel-bamboo composite column under axial compression. Engineering Mechanics 29: 221-225.
20. Xiao, Y., Li, L., Yang, R.Z., 2014: Long-term loading behavior of a full-scale glubam bridge model. Journal of Bridge Engineering 19(9): 04014027.
21. Xiao, Y., Zhou, Q., Shan, B., 2010: Design and construction of modern bamboo bridges. Journal of Bridge Engineering 15(5): 533-541.
22. Zhang, Z.W., Li, Y.S., Liu, R., 2015: An analytical model of stresses in adhesive bonded interface between steel and bamboo plywood. International Journal of Solids and Structures 52: 103-113.
23. Zhao, W.F., Qu, P., Zhou, J., Long, Z.L., 2016a: Axial compression behavior of square thin-walled steel tube/bamboo plywood composite hollow column with binding bars. Acta Materiae Compositae Sinica 33(10): 2325-2335.
24. Zhao, W.F., Zhou, J., Long, Z.J., Peng, W.X., 2018: Compression performance of thin-walled steel- tube/bamboo plywood composite columns with binding bars. Advance in Structural Engineering 21(3): 347-364.

25. Zhao, W.F., Zhou, J., Long, Z.L., 2016b: Compression tests on square, thin-walled steel tube/bamboo-plywood composite hollow columns. Science and Engineering of Composite Materials 23(5): 511-522.
26. Zhou, J., Chen, Z.S., Zhao, W.F., Yang, B., 2018: Axial compressive performance of thin-walled steel tube/bamboo-plywood composite hollow long column with binding bars. Chinese Journal of Applied Mechanics 35(3): 489-495.

Weifeng Zhao
Guangdong Construction Polytechnic
Guangzhou
China

Weifeng Zhao, Bin Yang
Xiangtan University
College of Civil Engineering and Mechanics
Xiangtan
China

*Jing Zhou
South China University of Technology
Key Laboratory of Subtropical Architecture Science
Guangzhou 510640
China
*Corresponding author: ctjzhou@scut.edu.cn
Phone number: +86-139-0228-8258